

Search and characterization of Satellite Galaxies and Stellar Streams of the Milky Way in the S-PLUS survey

P. Augusto Ré¹, F. Almeida-Fernandes^{1,2}, C. Mendes de Oliveira¹, & H. D. Perottoni¹

¹ Departamento de Astronomia, IAG, Universidade de São Paulo, Rua do Matão, São Paulo, Brasil

e-mail: pierre@usb.br, felipe.almeida.fernandes@usp.br, claudia.oliveira@iag.usp.br, hperottoni@gmail.com

² NSF's NOIRLab, 950 N. Cherry Ave., Tucson, AZ 85719, USA

Abstract. We present a methodology to search for new overdensities in the Milky Way with the isochronal filter technique. The overdensities, which in general are satellite galaxies accreted by the Milky Way, open the possibility of the study for a better understanding of the origin and evolution of our galaxy. Observing the various mergers that occurred until reaching the structure we see today, it is still predicted that new overdensities will still be found.

Data from the S-PLUS survey will be used, which makes observations in 12 photometric filters. The use of more photometric bands brings new findings, as we can separate data from nearby dwarf stars and distant giant stars, due to narrow filters, that are sensitive to the surface gravity. In addition, the new areas to be explored in the southern hemisphere sky, are promising within the search.

Thus, we apply to the data a technique already used in other works, which consists of using evolutionary isochrones to select the stars belonging to a certain population. However, with a differential, including probabilities of belonging to these populations. The calculated probabilities are considered in the construction of density maps to assign greater weight to the stars in the population.

Resumo. Apresentamos uma metodologia para busca de novas sobredensidades na Via Láctea com a técnica do filtro isocronal. As sobredensidades, que em geral são galáxias satélites acretaadas pela Via Láctea, abrem a possibilidade do estudo para melhor compreensão da origem e evolução da nossa galáxia. Observando as diversas fusões que ocorreram até chegar na estrutura que vemos hoje, sendo ainda previsto que novas sobredensidades ainda sejam encontradas.

Serão usados os dados do levantamento S-PLUS, que realiza observações em 12 filtros fotométricos. A utilização de mais bandas fotométricas trazem novos achados, já que podemos separar os dados de estrelas anãs próximas das gigantes distantes, devido aos filtros estreitos. Além disso, as novas áreas a serem exploradas do céu do hemisfério Sul, são promissoras dentro da busca.

Assim, aplicamos aos dados uma técnica já utilizada em outros trabalhos, que consiste em usar isócronas evolutivas para selecionar as estrelas pertencentes a uma determinada população. Porém, com um diferencial, incluindo probabilidades de pertencerem a essas populações. As probabilidades calculadas são consideradas na construção dos mapas de densidade para atribuir maior peso às estrelas da população.

Keywords. Galaxies: dwarf – Galaxies: structure

1. Introduction

One of the main objects to better understand the formation and evolution mechanism of the Milky Way, as well as its gravitational potential (Bonaca 2014), it's stellar overdensities. They are, in general, Satellite Galaxies accreted by our Galaxy (Newberg & Carlin 2016). After incorporation by gravitational interaction, the object's stars overlap the densities of local stars. Furthermore, the kinematics of stellar populations will refer directly to their ancient progenitor. Finding new satellites around the Milky Way helps us to study the low-luminosity limits of star formation (Koposov et al. 2007; Balbinot et al. 2013). Populations residing in the Milky Way include less luminous, less chemically enriched and more dark matter dominated galaxies in the known Universe (e.g. Simon & Geha 2007; Kirby et al. 2008). Thus, looking at emerging populations of near-field galaxies, allows a unique condition for testing galaxy formation models and studying the cold dark matter paradigm (e.g Bullock et al. 2001).

Most of the photometric surveys, such as Sloan Digital Sky Survey (SDSS) (York et al. 2000), changed the paradigm of the Milky Way satellites, revealing a large number of low-luminosity star systems, hitherto invisible (Willman et al. (2005; Irwin et al. 2007; Belokurov et al. 2007b; Walsh et al. 2007). Surveys such as Pan-STARRS, VST ATLAS, among others, also

contributed to the identification of new satellite galaxies (e.g. Laevens et al. 2015b,a; Torrealba et al. 2016).

Another extremely important and crucial survey for the search for new satellites was the Dark Energy Survey (DES) (The Dark Energy Survey Collaboration 2005). It allowed the discovery of at least more than 21 new Satellite Galaxies (e.g., Kim & Jerjen 2015; Bechtol et al. 2015; Koposov et al. 2015; Drlica-Wagner et al. 2015). In all, today we have an extensive list of more than 60 satellite galaxies around the Milky Way (Drlica-Wagner et al. 2020).

In these Milky Way substructures, discrepancy problems were presented in the predicted amount of dark matter subhalos, compared to satellite galaxies that should exist in the Milky Way's surroundings (cf. Moore et al. 1999; Klypin et al. 1999; Simon & Geha 2007). However, with the evolution of models of star formation in the less massive dark matter subhalos, the problem in the scale of missing objects has eased (e.g., Bullock & Johnston 2005). However, we still have a lower number of expected satellite galaxies compared to observed ones. Occurring due to some of these objects being too diffuse and faint to be easily found, the search then becomes limited to difficulties such as: The areas of the sky to be explored, the observational completeness and the sensitivity and optimizations in the search algorithms of the objects (Tollerud et al. 2008).

2. Sample

2.1. S-PLUS data release 4

The data used here is the internal data release 4 (iDR4) of the Southern Photometric Local Universe Survey (S-PLUS) (Mendes, C. L. et al. 2019), which comprises an area of ~ 9300 deg² of the sky, specifically the southern hemisphere of the celestial sphere. S-PLUS uses the 0.8m T-80 South robotic telescope at the Cerro Tololo Inter-American Observatory, Chile, where it covers twelve optical bands. Among the filters, with the Javalambre magnitude system, we have 5 broadband filters and 7 narrowband filters.

The data used here can be obtained from the *SplusData* library or from the *splus cloud* website (<https://splus.cloud>) through an ADQL Query. We applied the necessary extinction corrections for the 12 photometric bands, using Schlegel maps (Schlegel, Finkbeiner, & Davis 1998) to estimate the necessary correction in each telescope observation.

The previous cuts performed on the data were:

$s2n-Det-astro > 3$, selecting the objects with the highest noise signal. With $nDet-astro > 3$, we remove possible artifacts from the image, which is equivalent to considering only objects with detections in at least 3 filters. With $CLASS_STAR > 0.8$, we remove galaxies and select only stars.

2.2. Stellar isochrones

Evolutionary isochrones from the models Padova and Trieste Stellar Evolutionary Code (PARSEC) (Bressan et al. 2012) (<http://stev.oapd.inaf.it/cgi-bin/cmd>) were used. The set of isochrones used presents magnitudes in the photometric system of S-PLUS (in the Vega system), modified to *ABs* in the applications made.

2.3. Objects of study in the sample

Fields with known Satellite Galaxies in the Milky Way (Drlica Wagner et al. 2020) were selected within the S-PLUS data. We present in the Tab.1 the selected objects.

The values selected for metallicities and distances were obtained as estimates found in the references. Based on them, we obtained simulated isochrones with the same characteristics as the parameters. It should be noted that the values do not need to be exact, as tests will be simulated for specifications of characteristics close to the known Satellite Galaxies.

3. Methods

3.1. Isochronal filter method

With the narrow photometric filters of S-PLUS, specifically the F378 and F515, it is possible to distinguish the most distant giants from the nearby dwarfs. This is due to absorption lines sensitive to the surface gravity of these two types of stars, such as the magnesium triplet at ~ 515 nm. We obtain a sample with cuts in a color-color diagram, which select regions mostly occupied by giant stars.

The isochronal filter method was used after selecting the giant stars. This method is correlated with the positions of the stars in the HR Diagram. It is possible to apply this method to find, for example, the ages of individual stars or, mainly, of clusters. These clusters are formed by simple stellar populations, in which a set of stars are formed together with the same chemical compositions and ages. In this way, using stellar tracers, it is possible

to find isochrones that best represent that population, thus determining their characteristics. Therefore, the isochronal method is able to characterize the age, metallicity and distance of a cluster.

We know that, in addition to clusters, we can approximate Satellite Galaxies by these same simple stellar populations (e.g. Drlica-Wagner et al. 2015). In this way, we can use the evolutionary isochrones to search for possible populations with the same characteristics.

In a catalog containing mostly more giants, we can apply isochrones only to these same evolutionary branches. Giants have a higher intrinsic brightness and lower magnitudes. We will use them to search for more distant populations.

For each observation, we look for traces of a stellar population by selecting stars around a given isochrone. The stars are selected by applying a mask around the isochrones. In this study, we will be selecting the stars in these masks, according to the photometric errors of the 12 bands of the S-PLUS, estimating probabilities that each observed star belongs to that stellar population.

3.2. MaGIK program

An algorithm was developed, written in python language. The program is named MaGIK (Mapping Galaxies using Isochronal likelihood and KDE), written for SDSS and optimized for S-PLUS data.

First, the isochrones that will be applied are selected, considering an age and metallicity that will characterize the SSP that we will look for in the field.

With the isochronal likelihood filter technique, for each of the stars, we calculate the probabilities, given the photometric error of the magnitudes, of belonging to that stellar population. Due to errors, the stars may be shifted in the diagram, so with a Bayesian approach, these probabilities are inferred. Stars with large photometry errors are also cut out, so that the joint error of the Color used is less than 0.04.

Since we don't know how far the satellite galaxies are, we need to search for these objects in different ranges of distance. Thus, the process must be repeated for the same isochrone covering different distances.

We present an example in the Fig.1, of a test field with an isochrone applied, where we observe the probabilities calculated in this step through the color bar.

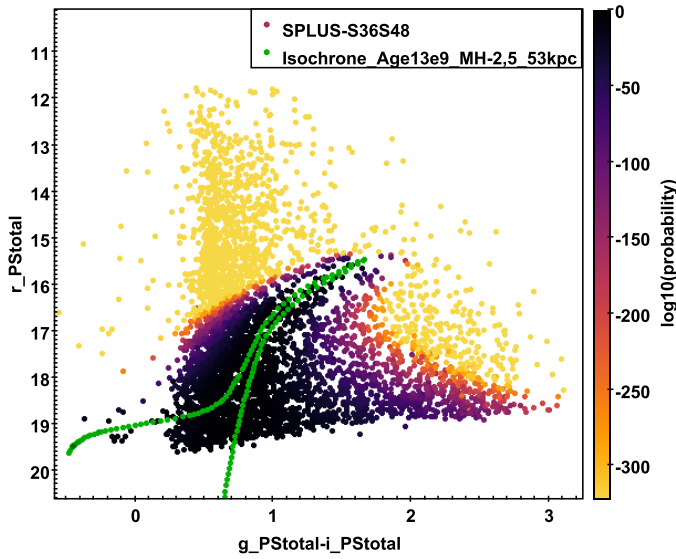
In the next step, the stars are subdivided into groups based on the percentiles of the probability distribution. In this way, we have a group from the lowest to the highest percentage of probabilities of stars belonging to the SSP. The stars in each percentile range have their spatial distribution transformed into a density map using the KDE (kernel density estimator) technique.

For this, the stars with a higher probability of belonging to the SSP are assigned a Gaussian kernel with a smaller area, and a greater height, in order to highlight the object's signal. For the stars of the lower probability groups, a larger kernel is assigned, with a Gaussian of greater area and therefore lower height, highlighting the stars at the bottom of the map. The Gaussians and each of the subgroups are summed, creating density maps with their heights of the levels given by the color. Each of the maps of the subgroups will be interpolated, creating the total density map of the applied field.

With the total map created, it is still necessary to normalize it. We must take into account that, for different regions of the sky, there must be discrepancies in the stars due to the density gradient of the different populations of the Galaxy. Due to the global density profile, certain parts of the map, even with low

TABLE 1. Satellite Galaxies present in the S-PLUS iDR4. Presented with their location in the sky (equatorial coordinates), distance in *kpc*, estimated metallicity $[Fe/H]$, field name in the S-PLUS survey, and the data reference

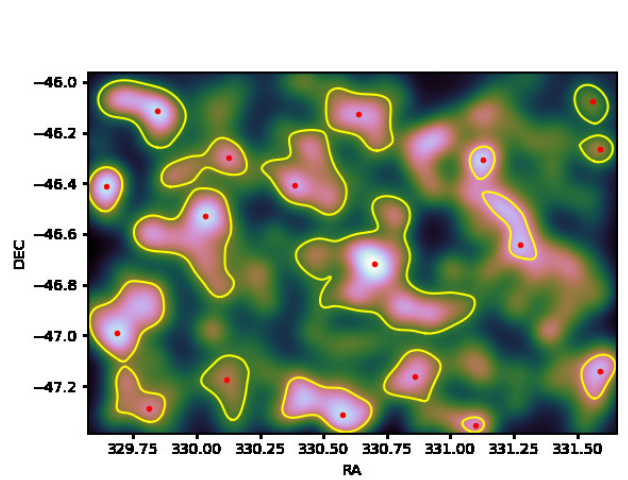
Name	Ra	Dec	Distance (kpc)	[Fe/H]	SPLUS field	Reference
Leo IV	173,2	-0,53	154	-2,36	SPLUS-n01s18	(Willman & Strader 2012)
Virgo I	180,0	-0,68	91,0	-2,2	SPLUS-n02s23	(Homma et al. 2016)
Crater II	177,14	-18,9	117,5	-1,7	SPLUS-n15s20	(Torrealba et al. 2016)
Sculptor	15,04	-33,7	80	-2,0	SPLUS-s26s10	(Leaman et al. 2012)
Fornax	39,45	-34,87	147	-1,02	SPLUS-s27s25	(Willman & Strader 2012)
Eridanus II	55,96	-44,07	370	-2,62	SPLUS-s34s31	(Koposov et al. 2015)
Grus II	330,65	-46,67	53	-2,51	SPLUS-s36s48	(Hansen et al. 2020)
Horologium II	49,1	-50,0	78	-2,1	SPLUS-s39s24	(Jerjen et al. 2018)
Pictor I	71,58	-50,56	114	-2,8	SPLUS-s39s35	(Jerjen et al. 2018)
Kim 2	317,2	-51,16	100,0	-1	SPLUS-s39s38	(Kim et al. 2015)
Reticulum II	53,92	-54,04	30	-2	SPLUS-s42s25	(Koposov et al. 2015)
Phoenix II	355,41	-54,43	83	-2,1	SPLUS-s42s51	(Jerjen et al. 2018)
Tucana II	342,97	-58,56	58	-2,23	SPLUS-s45s41	(Chititi et al. 2022)
Tucana III	0,02	-59,60	25	-2,5	SPLUS-s46s01	(Marshall et al. 2019)


FIGURE 1. Isochrone in green with Age 13 Gyr, metallicity -2.5 dex and distance of 53 kpc. Color-magnitude diagram (Color $g-i$, magnitude r , in S-PLUS magnitudes) colored according to the probability of stars belonging to the isochrone.

probability, may show a high value. Thus, the program generates the density map again, normalized according to the mean and the local standard deviation, showing better the local peaks. This is done by selecting for each pixel a ring around it, with 40 pixels, out of a total of 200 pixels for each field, in which the arc pixels are averaged, subtracting from the original central pixel.

Finally, we characterize the peaks in the normalized maps in order to differentiate between real detection and noise fluctuations. Which do not necessarily correspond to a distinct stellar population. Local maximums are selected on the maps, given a certain distance in pixels in the configuration file. For each of the selected points, contours are created on the levels around the maxima. We characterize its scattering according to the area of the lowest level contour, which includes just that peak. With this application, the best selected contours are superimposed on the map. Shown in Fig.2 is an example of the normalized total density map, with its local maxima and contours selected for an S-PLUS field.

Graphs are also created with the parameters of the area and depth (difference between the height of the local maximum and


FIGURE 2. Total normalized density map. Red dots correspond to selected local maximums, with characterized yellow contours created.

the level of its characterized contour), in which we can identify the possible populations for each field. As the analysis will be repeated with many isochrones for the same field (different ages, metallicities and distances), and even slightly different isochrones are able to highlight a given population, it is possible that real populations can be detected multiple times.

It should also be noted that, in order to observe a detection and classify it as a possible population, we need to apply the methodology for control fields. These fields will be used in regions that where no Galactic overdensities are known. Thus, if we find detections above a certain cutoff in area and depth, when compared to the control fields, we can classify them as a possible detection.

4. Results

4.1. Detection of galaxies in single and multiple fields

To test the parameters used in MaGIK, as proposed, the code was applied to the known Satellite Galaxies in the Milky Way within the S-PLUS (Tab.1). First, the result is made for the Sculptor galaxy, as it is a population with relatively more stars, and therefore easier to be evidenced.

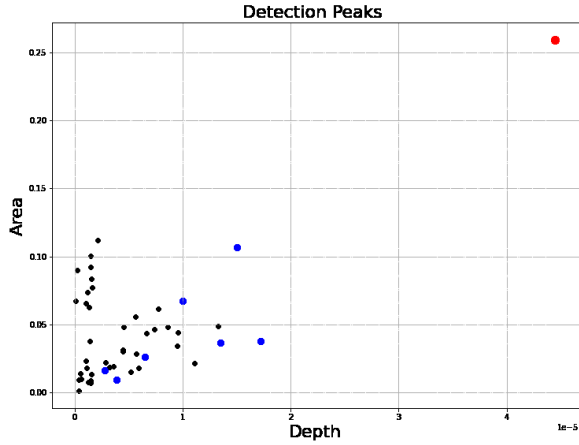


FIGURE 3. Detection graph for the SPLUS-s26s10 field. Points in blue associated with each of the local maximums of the background of the density map created for the region. Black dots are local maximums for control fields, at locations with no expected detections. The red dot corresponds to the detection of the Sculptor galaxy.

An isochrone of the same characteristics expected for the population was applied in the *SPLUS-s26s10* field. We present in Fig.3 the result of the field detection graph, together with the detections used for the control fields. Note that the lowest points on the left correspond to the noise fluctuation of the density map (as evidenced by the control field), without corresponding to a possible population. The most prominent point on the upper right, with a large area and depth, is correlated with Sculptor detection, with values above the control fields.

One of the objectives, in addition to the Satellite Galaxies, is to observe if it is possible to evidence Stellar Streams. They are more diffuse and elongated, thus occupying a greater area of the sky. Therefore, it is necessary to cover more than one field simultaneously to view them.

Different numbers of fields were concatenated around Sculptor, with combinations of two, three and eight fields. Thus, we want to show that even with more fields, the existing population in them will still be evidenced. In Fig.4, we show the result of the detection graph of the concatenated regions.

It is observed how the detection graph follows a similar trend for each of the options. Which is to be expected, as they all have Sculptor present for detections. For the points on the lower left, we have the detections from the bottom of the map, while for the points on the upper right, we have the population highlighted.

4.2. Analysis for known galaxies in the Milky Way

To analyze the parameters used within MaGIK, we need to test on known objects. So, if we show the best parameters that evidence the known Galaxies, we can test them in new regions. In Tab.1, we show the satellite galaxies within the S-PLUS iDR4. Applying evolutionary isochrones of the same characteristics of each galaxy, all the processes presented within the MaGIK code were carried out. We present in Fig.5 the result of the detection graph for all satellite galaxies, together with results for the control fields.

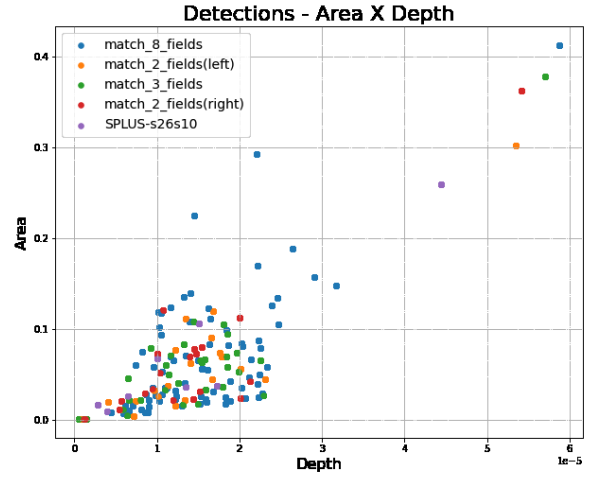


FIGURE 4. Detection graphic for Sculptor galaxy. Each color represents a combination of fields that includes the Galaxy in its data. On the upper right, we have the dots that represent Sculptor detection.

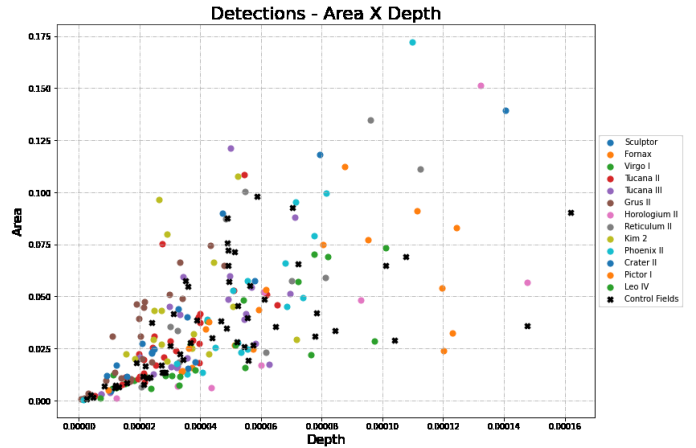


FIGURE 5. Graph of detections for testing Satellite Galaxies in the Milky Way with S-PLUS data. Colored dots represent detections from Galaxies, black dots from control fields of expected regions without detection.

5. Conclusions

The search for new overdensities is influenced by the selected filters, with the redder filters being able to detect stars with fainter magnitudes and, therefore, reaching deeper observed distances.

With the addition of features in the MaGIK program, we were able to identify the signature of known satellite galaxies. Furthermore, we show that it is possible to highlight Satellite Galaxies both in individual fields and in multiple concatenated fields. In this way, we can apply MaGIK to large areas, looking for Stellar Streams.

For Satellite Galaxies with a higher density of stars, we found detections that stood out from control fields (fields without known satellite galaxies).

References

Mendes, C. L. et al., 2019, Monthly Notices of the Royal Astronomical Society, 489:241–267.

- Schlegel, D. J., Finkbeiner, D. P., & Davis, M., 1998, *The Astrophysical Journal*, 500(2):525–553.
- Bressan, A. et al., 2012, *Monthly Notices of the Royal Astronomical Society*, 427(1):127–145.
- Drlica-Wagner, A. et al., 2020, *The Astrophysical Journal* 893(1):47.
- Willman, B. & Strader, J., 2012, *The Astronomical Journal*, 144(3):76.
- Homma, D. et al., 2016 *The Astrophysical Journal*, 832(1):21.
- Torrealba, G. et al., 2016, *Monthly Notices of the Royal Astronomical Society*, 459(3):2370–2378.
- Leaman, R. et al., 2012, *The Astronomical Journal*, 144(6):183.
- Hansen, T. T. et al., 2020, *The Astrophysical Journal*, 897(2):183.
- Jerjen, H. et al., 2018, *Monthly Notices of the Royal Astronomical Society*.
- Kim, D. et al., 2015, *The Astrophysical Journal*, 803(2):63.
- Koposov, S. E. et al., 2015, *The Astrophysical Journal*, 805(2):130.
- Chiti, A. et al., 2022, *The Astrophysical Journal*, 857(1)
- Marshall, J. L. et al, 2019, *The Astrophysical Journal*, 882(2):177.
- Newberg, H. J. & Carlin, J. L., 2016, *Tidal Streams in the Local Group and Beyond Observations and Implications*, volume 420. Springer, 3 edition.
- Koposov, S. et al., 2007, *The Astrophysical Journal*, 669(1):337.
- Balbinot, E. et al., 2013, *The Astrophysical Journal*, 767(2):101.
- Simon, J. D. & Geha, M., 2007, *The Astrophysical Journal*, 670(1):313–331.
- Kirby, E. N. et al., 2008, *The Astrophysical Journal*, 685(1):L43–L46.
- Bullock, J. S., Kravtsov, A. V., & Weinberg, D. H., 2001, *The Astrophysical Journal*, 548(1):33–46.
- York, D. G. et al., 2000, *American Astronomical Society*, 120(3), 1579–1587.
- Willman, B. et al., 2005, *The Astronomical Journal*, 129(6):2692–2700.
- Irwin, M. J. et al., 2007, *The Astrophysical Journal*, 656(1):L13–L16.
- Belokurov, V. et al., 2007, *The Astrophysical Journal*, 657(2):L89–L92.
- Walsh, S. M., Jerjen, H., & Willman, B., 2007, *The Astrophysical Journal*, 662(2):L83–L86.
- Laevens, B. P. M. et al., 2015, *The Astrophysical Journal*, 813(1):44.
- Laevens, B. P. M. et al., 2015, *The Astrophysical Journal*, 802(2):L18.
- Torrealba, G. et al., 2016, *Monthly Notices of the Royal Astronomical Society*, 459(3):2370–2378.
- The Dark Energy Survey Collaboration, 2005, eprint arXiv:astro-ph/0510346.
- Kim, D. & Jerjen, H., 2015, *The Astrophysical Journal*, 808(2):L39.
- Bechtol, K. et al., 2015, *The Astrophysical Journal*, 807(1):50.
- Koposov, S. E. et al., 2015, *The Astrophysical Journal*, 805(2):130.
- Drlica-Wagner, A. et al., 2015, *The Astrophysical Journal*, 813(2):109.
- Drlica-Wagner, A. et al., 2020, *The Astrophysical Journal*, 893(1):47.
- Moore, B. et al., 1999, *The Astrophysical Journal*, 524(1):L19–L22.
- Klypin, A. et al., 1999, *The Astrophysical Journal*, 522(1):82–92.
- Simon, J. D., & Geha, M., 2007, *The Astrophysical Journal*, 670(1):313–331.
- Bullock, J. S., & Johnston, K. V., 2005, *The Astrophysical Journal*, 635(2):931–949.
- Tollerud, E. J. et al., 2008, *The Astrophysical Journal*, 688(1):277–289.